Appl. Phys. B 70, 33–43 (2000) / Digital Object Identifier (DOI) 10.1007/s003409900136

Applied Physics B
Lasers
and Optics

General model for a multimode Nd-doped fiber laser. II: Steady-state analysis of length-dependent polarization effects

T. Chartier[1], **F. Sanchez**[1], **G. Stéphan**[2]

[1] Groupe d'Optique et d'Optronique, CORIA UMR 6614, Université de Rouen, Place Emile Blondel, 76821 Mont-Saint-Aignan Cedex, France
(Fax: +33-2/3570-8384, E-mail: name@coria.fr)
[2] ENSSAT, Laboratoire d'Optronique, équipe associée au CNRS (UPRESA 6082), 6, rue de Kérampont, B.P.447, 22305 Lannion Cedex, France
(Fax: +33-2/9637-0199, E-mail: stephan@enssat.fr)

Received: 9 November 1998/Revised version: 26 April 1999/Published online: 30 November 1999

Abstract. We present a steady-state analysis of a general model for a bipolarized Nd-doped fiber laser including the slow longitudinal variations of the dynamical variables. The combined effects of pump-induced, distributed, and localized anisotropies are studied versus the fiber length. In particular, the evolution of the thresholds versus the pump-input polarization angle, for different fiber lengths, is investigated in depth. Approximate analytical results are derived for the thresholds and the output intensities. A good agreement with the numerical simulations is achieved in a large range of parameters.

PACS: 42.55.Wd; 42.25.Ja; 42.55.Ah

The simplest model for a single-mode laser, owing to the fast relaxation of the medium polarization (class-B laser), reduces to two rate equations [1]: one for the population inversion and the other for the laser intensity. A different approach, originally described by Rigrod in 1963 [2], consists in taking into account the forward and the backward fields inside the cavity. This early model includes the longitudinal variations of the laser field along the resonant cavity (z axis) and allows to introduce localized losses (mirrors or others), distributed losses, and inhomogeneous pumping. The rate equations are obtained using the mean-field approximation in which the laser properties as well as dynamical variables are averaged along the cavity and by assuming that the forward and the backward fields are z-independent. Rigrod's model can be adapted to diode-pumped solid-state lasers where the longitudinal pumping leads to an unsaturated gain decreasing along the cavity. This model has been used for the study of the steady-state properties of solid-state lasers, doped superfluorescent fibers and fiber lasers [3–5]. The major inconvenience of this approach is that, in general, it does not lead to analytical results. However it has the advantage of describing the slow variations of the fields along the amplifying medium and of taking into account both inhomogeneous (distributed) and localized phenomena.

There are now numerous theoretical works on bimode lasers dynamics [6–14], and in particular, on bipolarized lasers. See for instance the frequency-doubled Nd:YAG laser [6], VCSEL [7, 8], and Nd-doped fiber lasers [9, 10]. Most of these theories are oriented toward the study of the temporal evolution of the system and not the spatial aspect. Indeed, whether or not, the optical coherence is taken into account, the z-dependence of the fields is ignored. This approach is however justified when the interest lies only in the temporal evolution of the laser for a given configuration, i.e. for fixed values of both the active medium length and the reflection coefficient of the mirrors. However under such conditions, the steady-state description of the system, in particular the influence of either localized or distributed parameters (losses, gain, polarization-dependent loss), cannot be complete and thus the theory cannot be predictive.

In the case of fiber lasers, the fiber length can be considered as a control parameter since it can be easily changed [4, 15]. Moreover, diode end-pumping leads to an unsaturated gain which varies along the fiber length. Therefore, length-dependent steady-state properties deserve a particular attention. In the previous paper we have derived a general model for the Nd-doped fiber laser which keeps the slow variations of the dynamical variables both in time and along the longitudinal coordinate [16]. The model assumes a linearly polarized pump-field interacting with randomly distributed anisotropic dipoles. The output intensity consists of two groups of modes linearly polarized along the eigenaxis of the doped fiber. These modes have a random phase with respect to each other and, under the mean-field approximation, the model reduces to classical bipolarized laser equations which allows for dynamical studies [9, 10, 17]. Hereafter the term of *mode* will be devoted to the polarization modes of the laser. At steady-state, the general model is a generalization of the Rigrod's theory to the case of a bipolarized laser. It is very useful to investigate combined effects of length, localized, and distributed polarization-dependent loss or gain on the steady-state properties of a fiber laser. The aim of this paper is to propose an approximate analytical solution at steady-state to our general model. This solution allows us to establish the *operating regime diagram* which offers a synthetic view of the different regimes characterizing a bipolarized laser and to investigate length-dependent polarization effects.

The general model is briefly presented in Sect. 1. It takes into account: (i) the forward and the backward intensities inside the cavity, (ii) both localized and distributed losses, and (iii) both localized and distributed loss anisotropies. We are only interested in the steady-state analysis of the problem. Section 2 is devoted to the study of the single-mode (scalar) case. As mentioned above, even in the single-mode case there is no analytical solution to the problem. We propose here an approximation that yields closed-form expression for the output intensity of the laser in all cases investigated, i.e. single-mode and two-mode (vectorial) cases. The assumption consists in considering that the total intensity inside the cavity is z-independent whereas the forward and backward intensities are z-dependent. The validity of this approximation is determined by a direct comparison with exact numerical results. The bipolarized model is investigated in Sect. 3. Approximate analytical results for the output intensities are obtained in all cases of interest. As in Sect. 2, a direct comparison of analytical and numerical solutions is made. The combined effects of pump-polarization angle and fiber length on the thresholds of the two modes are further studied.

1 The general model

In the previous paper [16], we have derived a general model for a bipolarized fiber laser that keeps the temporal and longitudinal slow variations of the fields. A schematic representation of the system under study is given in Fig. 1. We consider a Fabry–Pérot cavity which supports two counterpropagating fields. Each of them is decomposed on the basis of the eigenaxis of the fiber X and Y. The unsaturated gain is assumed to be exponentially decreasing along the fiber. This is equivalent to considering a non-saturated pump transition. At steady state, the equations for the normalized intensities are:

$$\pm\frac{\partial I_x^{\pm}}{\partial z} = -\kappa_x I_x^{\pm} + \frac{1}{2}\left(\frac{(1+\delta)\Lambda \mathrm{e}^{-\alpha z}}{1+I_x^{+}+I_x^{-}+\beta'(I_y^{+}+I_y^{-})} + \beta'\frac{(1-\delta)\Lambda \mathrm{e}^{-\alpha z}}{1+\beta'(I_x^{+}+I_x^{-})+I_y^{+}+I_y^{-}}\right) I_x^{\pm}, \tag{1a}$$

$$\pm\frac{\partial I_y^{\pm}}{\partial z} = -\kappa_y I_y^{\pm} + \frac{1}{2}\left(\frac{(1-\delta)\Lambda \mathrm{e}^{-\alpha z}}{1+\beta'(I_x^{+}+I_x^{-})+I_y^{+}+I_y^{-}} + \beta'\frac{(1+\delta)\Lambda \mathrm{e}^{-\alpha z}}{1+I_x^{+}+I_x^{-}+\beta'(I_y^{+}+I_y^{-})}\right) I_y^{\pm}. \tag{1b}$$

The superscript $+(-)$ means for the forward (backward) laser field component. $\kappa_{x,y}$ are the damping coefficients for the intensities associated with the X and Y field components. Λ represents the pumping parameter (normalized pump-input intensity), α the pump absorption coefficient, β' the cross-saturation parameter between the X and Y polarizations of the laser field, and δ the parameter associated with the pump-induced gain anisotropy, which we will call the gain anisotropy. β' is a measure of the microscopic anisotropy of the dipole [10]. In the following we shall be interested in linear pump polarization. In this case the gain anisotropy takes the form [16]:

$$\delta = \epsilon\cos 2\phi_0 = \frac{1-\beta}{1+\beta}\cos 2\phi_0\,, \tag{2}$$

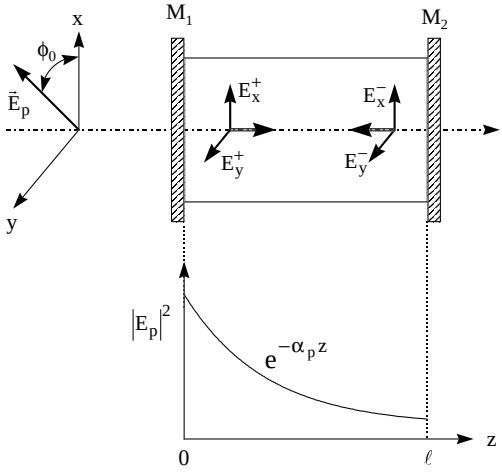

Fig. 1. Schematic representation of the problem

where ϕ_0 is the angle between the pump-input polarization and the x axis (Fig. 1) and β the cross-saturation parameter for the pump field. The damping coefficients are written:

$$\kappa_x = \kappa(1-\gamma)\,,$$

$$\kappa_y = \kappa(1+\gamma)\,,$$

where γ is the distributed loss anisotropy. Together with γ, the model allows us to introduce localized loss anisotropies, especially on the mirrors. The boundary conditions on the mirrors are:

$$\begin{aligned} I_x^{+}(0) &= R_1^x I_x^{-}(0), \qquad I_y^{+}(0) = R_1^y I_y^{-}(0)\,,\\ I_x^{-}(l) &= R_2^x I_x^{+}(l), \qquad I_y^{-}(l) = R_2^y I_y^{+}(l)\,. \end{aligned} \tag{3}$$

The reflection coefficients are written:

$$\begin{aligned} R_{1x} &= (1+t_1)R_1, \qquad R_{1y} = (1-t_1)R_1\,,\\ R_{2x} &= (1+t_2)R_2, \qquad R_{2y} = (1-t_2)R_2\,, \end{aligned} \tag{4}$$

where $t_{1,2}$ are localized loss anisotropies on the mirrors and $R_{1,2}$ the average reflection coefficients.

2 Analysis of the single-mode model

In order to simplify our analysis, we may first consider the single-mode case, i.e. when polarization properties of the laser are not taken into account. This simpler model can be deduced from the general model by assuming that $I_x^{\pm} = I_y^{\pm}$ and writing the new system for the variable $I^{\pm} = (1+\beta')/2\left[I_x^{\pm}+I_y^{\pm}\right]$ after having normalized z and κ respectively by $(1+\beta')/2$ and $2/(1+\beta')$. System (1) reduces to :

$$\frac{\partial I^{\pm}}{\partial z} = \pm\left(\frac{\Lambda \mathrm{e}^{-\alpha z}}{1+I^{+}+I^{-}} - \kappa\right) I^{\pm}\,. \tag{5}$$

The boundary conditions on the mirrors become:

$$I^{+}(0) = R_1 I^{-}(0)\,, \tag{6a}$$

$$I^{-}(l) = R_2 I^{+}(l)\,. \tag{6b}$$

Basically, (5) is the set of equations studied by Rigrod at the early stage of laser physics [2]. The difference is that, in our case, we consider longitudinal variations of the unsaturated gain resulting from the pump absorption mechanism. Note that system (5) with constraint (6) does not admit any analytical solution. Our aim in this section is not to reproduce the analysis of Rigrod but rather to consider a simple case in order to derive approximate analytical solutions and to determine the range of validity of our assumption which will be used for the analysis of the general model.

Let us introduce normalized variables:

$$z' = \kappa z, \qquad \alpha' = \frac{\alpha}{\kappa}, \qquad \Lambda' = \frac{\Lambda}{\kappa}.$$

The saturated gain can be expressed as:

$$G(z) = \frac{\Lambda \mathrm{e}^{-\alpha z}}{1 + I^+ + I^-}$$

where the primes have been omitted in order to simplify the notations. The exact expression of the threshold can be easily obtained by equalizing the total losses to the unsaturated gain integrated over one round-trip in the cavity (oscillation condition). Its expression is:

$$\Lambda^{\mathrm{th}} = \frac{\alpha l}{1 - \mathrm{e}^{-\alpha l}} \left(1 - \frac{1}{2l} \ln R_1 R_2 \right). \tag{7}$$

2.1 Numerical simulations

Before considering the analytic development, we give some numerical solutions of system (5) which will be useful to justify our assumption. Figure 2 represents the evolution of the intensities $I^{\pm}(z)$ along the cavity together with the local average intensity defined as $I(z) = (I^+(z) + I^-(z))/2$. Three different normalized lengths are considered: (a) $l = 0.01$, (b) $l = 0.1$, and (c) $l = 1$. The parameters used for this calculation are: $R_1 = 1$, $R_2 = 0.8$, $\alpha = 100$, and $\Lambda = 200$. This means that, for physical values of $\kappa = 0.01\,\mathrm{m}^{-1}$ (43 dB/km) and $\alpha = 1\,\mathrm{m}^{-1}$ (4.3 dB/m) (which are realistic values for a 500-ppm Nd-doped fiber, for example), the real lengths, used in the calculation, are: 1 m, 10 m, and 100 m.

For the case (a) the fields are amplified within the whole fiber length, whereas for cases (b) and (c) the forward (backward) intensity exhibits a maximum (minimum) resulting from the combined effects of the decreasing unsaturated gain and the distributed losses. Indeed, for short lengths the saturated gain is locally higher than the losses along the whole fiber while for higher lengths, the saturated gain becomes locally lower than the losses beyond a particular propagating length. Moreover, the results of Fig. 2 show that the local average intensity remains practically constant over the fiber length excepting case (c).

2.2 Analytical results

This fact suggests we assume that the local average intensity is uniform along the fiber:

$$I = I^+(z) + I^-(z) = \text{constant}$$

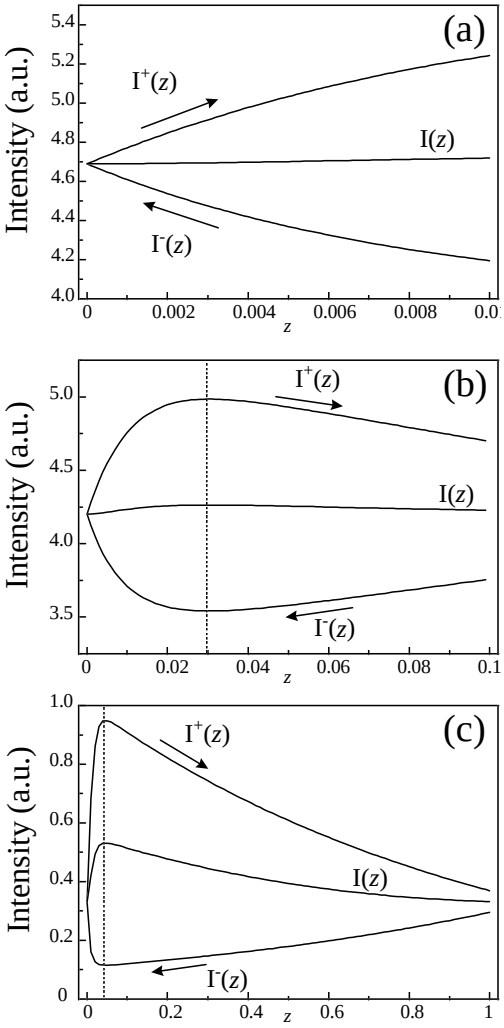

Fig. 2. Evolution of the forward ($I^+(z)$) and backward ($I^-(z)$) intensities together with the local average intensity ($I(z)$) along the cavity in the single-mode case and for different fiber lengths (see text). The parameters used are: $R_1 = 1$, $R_2 = 0.8$, $\alpha = 100$ and $\Lambda = 200$

Note that this hypothesis is less restrictive than the mean-field approximation [3, 19] since the latter requires that $I^+(z) = I^-(z) =$ constant. In addition, this approximation should be, a priori, good for short medium lengths (see Fig. 2a,b). The saturated gain becomes:

$$G(z) = \frac{\Lambda \mathrm{e}^{-\alpha z}}{1 + I}. \tag{8}$$

It is well known that in homogeneously broadened systems, the total gain does not depend on the pumping parameter above threshold [1], that means:

$$\frac{\partial}{\partial \Lambda} \int_0^l G(z)\,\mathrm{d}z = 0. \tag{9}$$

Integrating (8) along the fiber length and taking into account relation (9) yields:

$$\frac{1 + I - \Lambda \frac{\mathrm{d}I}{\mathrm{d}\Lambda}}{(1+I)^2} \left(\frac{1 - \mathrm{e}^{-\alpha l}}{\alpha} \right) = 0. \tag{10}$$

Equation (10) becomes:

$$\frac{\mathrm{d}I}{\mathrm{d}\Lambda} = \frac{1+I}{\Lambda} \,. \tag{11}$$

Using the fact that the intensity vanishes at threshold, the solution of (11) is:

$$I = \frac{\Lambda}{\Lambda^{\mathrm{th}}} - 1 \,, \tag{12}$$

where the threshold is given by (7).

Relation (12) is valid at any z, in particular at at $z = l$, and, using the boundary condition (6), the output intensity can be calculated:

$$I = I^{+}(l) + I^{-}(l) = (1+R_2)I^{+}(l) \,,$$

$$I^{\mathrm{out}}(l) = (1-R_2)I^{+}(l) \,.$$

Hence, the output intensity is:

$$I^{\mathrm{out}}(l) = \frac{1-R_2}{1+R_2}\left(\frac{\Lambda}{\Lambda^{\mathrm{th}}} - 1\right) \,. \tag{13}$$

Relation (13) contains the factor $1/(1+R_2)$ which does not appear in the mean-field approximation where it is replaced by $1/2$ which is the value of the previous factor with $R_2 = 1$. We find the well-known result that the mean-field approximation holds only for good optical cavity.

2.3 Validity of the analytical solution

The analytical expression of $I^{\mathrm{out}}(l)$ is a linear function versus the pumping parameter. The approximate analytical expression differs from the exact numerical solution only by the slope of the output intensity. Let us define an error function, $\Delta\epsilon$, which represents the relative shift between the two slopes. $\Delta\epsilon$ depends on the parameters α, l, and R_2. For a fixed pumping rate, the error function is given by:

$$\Delta\epsilon_{\alpha}(l,\, R_2) = \frac{I_{\mathrm{n}}^{\mathrm{out}}(l) - I_{\mathrm{a}}^{\mathrm{out}}(l)}{I_{\mathrm{n}}^{\mathrm{out}}(l)}$$

where the superscripts n and a respectively mean numerical and analytical solutions.

We arbitrarily consider that for a given set of parameters $(\alpha, l,\, R_2)$, there is a good agreement if $|\Delta\epsilon_{\alpha}(l,\, R_2)| \leq 0.1$ and a very good agreement if $|\Delta\epsilon_{\alpha}(l,\, R_2)| \leq 0.01$. Numerical studies of $\Delta\epsilon_{\alpha}(l,\, R_2)$ show that for any value of the pump absorption coefficient α, there exists a zone, included between the curves $l = f(R_2)$ solutions of $\Delta\epsilon_0(l,\, R_2) = -0.1$ and $\Delta\epsilon_{100}(l,\, R_2) = 0.1$, for which the shift between the analytical and numerical results is always below 10%. In the same manner, we can define a range for which the error function does not exceed 1%. Figure 3 summaries these studies and represents the range of validity for a good and a very good agreement, in the plane $(l,\, R_2)$. These results demonstrate that whatever the value of α, there exists couples $(l,\, R_2)$ for which the assumption, allowing analytical results to be obtained, is valid with a good accuracy.

Let us now compare directly the analytical and numerical results. Figure 4a shows the evolution of the output intensity

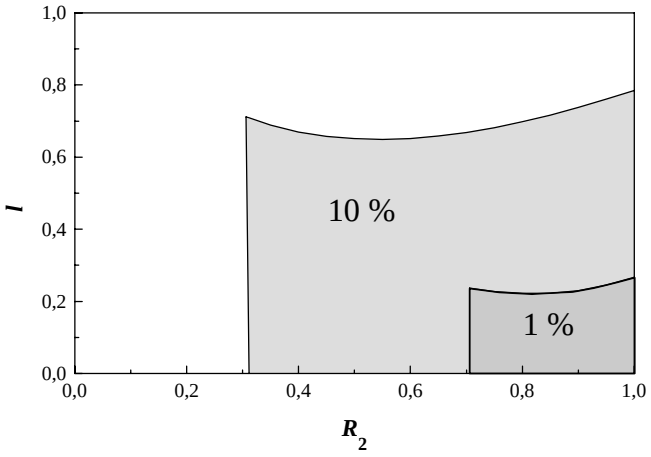

Fig. 3. Validity of the analytic solutions in the plane $(l,\, R_2)$, whatever α

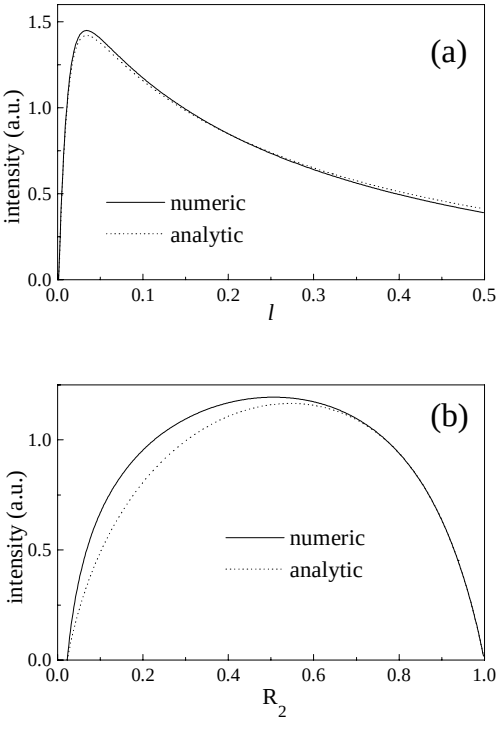

Fig. 4. **a** $I^{\mathrm{out}} = f(l)$ analytic (*dotted*) and numerical (*solid*) solutions with $R_2 = 0.8$. **b** $I^{\mathrm{out}} = f(R_2)$ analytic (*dotted*) and numerical (*solid*) solutions with $l = 0.1$, $R_1 = 1$, $\alpha = 100$, and $\Lambda = 200$

as a function of the fiber length for the same normalized (and physical) parameters as previously. The approximate analytical results (dotted curve) are very close to the exact numerical solution (solid line), especially for short fiber lengths which is in agreement with what was previously expected. Moreover, there exists an optimum value for the fiber length. This is directly connected with the existence of a minimum for the laser threshold [5]. Similar results have been reported for cw end-pumped lasers [20]. The evolution of the output intensity versus the output mirror reflectivity is given in Fig. 4b for $l = 0.1$. In this case, the agreement is good for high reflection coefficients.

At this stage of our study, it would be easy to analyze the influence of the fiber length on the optimum output-

coupling. This is not the purpose of this paper, and, moreover, it has been already investigated theoretically [21, 22] and experimentally [5]. However, let us recall the main result: for long and high-gain lasers, such as fiber lasers and particularly double-clad fiber lasers, the optimum output coupling ($T^{\text{opt}} = 1 - R_2^{\text{opt}}$) is relatively high (over 96%). This means that the output mirror reflectivity R_2 must be very low. This is connected to the important background losses that occur in this kind of lasers. Thus, our approximate solution is not adapted for fiber lasers which are used to reach maximum output power. However, it is worthwhile to point out that the exact numerical solution remains very helpful for these lasers and that not all fiber lasers attempt to achieve high power. High reflectivity of the output mirror can be used for example to reduce threshold for more fundamental studies.

In summary, the study of the well-known single-mode case has allowed us to define the range of validity for which both the analytical results and the assumption used are valid. In the following section we will restrict the analytical study of the general model to the range of parameters for which the assumption can be used with a good approximation.

3 Analysis of the general model

In this section we are interested in finding approximate analytical solutions to the general problem. The influence of the fiber length on the thresholds evolution versus the pump polarization angle is also investigated in depth and discussed.

The general equations, normalized exactly as in the previous section, can be written:

$$\frac{\partial I_x^{\pm}}{\partial z} = \pm \left(G_x(z) - 1 + \gamma\right) I_x^{\pm}\,, \tag{14a}$$

$$\frac{\partial I_y^{\pm}}{\partial z} = \pm \left(G_y(z) - 1 - \gamma\right) I_y^{\pm}\,. \tag{14b}$$

where:

$$G_x(z) = \frac{1}{2}\frac{(1+\delta)\Lambda \mathrm{e}^{-\alpha z}}{1 + I_x^+ + I_x^- + \beta'(I_y^+ + I_y^-)} + \frac{1}{2}\beta'\frac{(1-\delta)\Lambda \mathrm{e}^{-\alpha z}}{1 + \beta'(I_x^+ + I_x^-) + I_y^+ + I_y^-}\,, \tag{15a}$$

$$G_y(z) = \frac{1}{2}\frac{(1-\delta)\Lambda \mathrm{e}^{-\alpha z}}{1 + \beta'(I_x^+ + I_x^-) + I_y^+ + I_y^-} + \frac{1}{2}\beta'\frac{(1+\delta)\Lambda \mathrm{e}^{-\alpha z}}{1 + I_x^+ + I_x^- + \beta'(I_y^+ + I_y^-)}\,. \tag{15b}$$

$G_{x,y}(z)$ represent the saturated gains experienced by the two polarized eigenmodes. At this stage we do not give the numerical solutions of system (14) but a direct comparison with the analytical results will be done throughout this section. As previously mentioned the parameters used in this section lie in the range of validity of our hypothesis.

The different anisotropies introduced in our model (gain: δ, distributed loss: γ, localized loss: $t_{1,2}$) lead to a loss of symmetry between the modes X and Y. In particular, their respective thresholds Λ_x^{th} and Λ_y^{th} are often different and depend upon the respective values of the anisotropies, so the first lasing mode (strong mode) can be polarized either along x or y and the second lasing mode (weak mode) can be polarized either along y or x. therefore, we have to distinguish several cases of interest [10, 11]:

- strong mode X:
  - $\Lambda_x^{\text{th}} < \Lambda < \Lambda_y^{\text{th}} \Rightarrow I_x \neq 0$ and $I_y = 0$,
  - $\Lambda > \Lambda_y^{\text{th}} \Rightarrow I_x \neq 0$ and $I_y \neq 0$.
- strong mode Y:
  - $\Lambda_y^{\text{th}} < \Lambda < \Lambda_x^{\text{th}} \Rightarrow I_y \neq 0$ and $I_x = 0$,
  - $\Lambda > \Lambda_x^{\text{th}} \Rightarrow I_y \neq 0$ and $I_x \neq 0$.

In the following we first assume, without loss of generality, that the strong mode is polarized along the x axis. In appendix C we will give a summary of analytical results in all cases.

3.1 Single-mode solutions: $\Lambda_x^{\text{th}} < \Lambda < \Lambda_y^{\text{th}}$

We assume here that the strong mode is polarized along the x axis. The range of parameters for which this is true will be determined later. Let us first evaluate the threshold for the X mode starting from the oscillation condition which writes

$$R_{1x}R_{2x}\exp\left[2\int_0^l \left(\left(1+\delta+\beta'(1-\delta)\right)\frac{\Lambda_x^{\text{th}}}{2}\mathrm{e}^{-\alpha z} - 1 + \gamma\right)\mathrm{d}z\right] = 1\,. \tag{16}$$

The threshold is straightforwardly calculated from (16) and takes the form:

$$\Lambda_x^{\text{th}} = \frac{2}{1+\beta'+\delta(1-\beta')}\frac{\alpha l}{1-\mathrm{e}^{-\alpha l}} \times \left[(1-\gamma) - \frac{1}{2l}\ln\left[(1+t_1)(1+t_2)R_1R_2\right]\right]. \tag{17}$$

Let us define

$$\epsilon' = \frac{1-\beta'}{1+\beta'}\,, \tag{18a}$$

$$L_{\text{p}} = \frac{\alpha l}{1-\mathrm{e}^{-\alpha l}}\,, \tag{18b}$$

$$\Gamma_x = (1-\gamma) - \frac{1}{2l}\ln\left[(1+t_1)(1+t_2)R_1R_2\right]\,, \tag{18c}$$

where Γ_x represents the total losses for mode X. Using (18), relation (17) can be written in condensed form as

$$\Lambda_x^{\text{th}} = L_{\text{p}}\Gamma_x\frac{1+\epsilon'}{1+\delta\epsilon'}\,. \tag{19}$$

Note that (19) is the exact expression of the threshold associated with the strong mode. In order to find an analytical expression for the output intensity, again we assume that

$$I_x = I_x^+(z) + I_x^-(z) = \text{constant}\,.$$

The saturated gain experienced by the X mode can be written:

$$G_x(z) = \frac{1}{2}\frac{(1+\delta)\Lambda \mathrm{e}^{-\alpha z}}{1+I_x} + \frac{1}{2}\beta'\frac{(1-\delta)\Lambda \mathrm{e}^{-\alpha z}}{1+\beta' I_x}\,.$$

We follow now the same procedure as that used in the previous section. The derivative of the saturated gain versus the pump parameter is:

$$\frac{\mathrm{d}G_x(z)}{\mathrm{d}\mathcal{A}} = \frac{1+\delta}{2}\frac{1+I_x-\mathcal{A}\frac{\mathrm{d}I_x}{\mathrm{d}\mathcal{A}}}{(1+I_x)^2}\mathrm{e}^{-\alpha z} + \beta'\frac{1-\delta}{2}\frac{1+\beta' I_x-\beta'\mathcal{A}\frac{\mathrm{d}I_x}{\mathrm{d}\mathcal{A}}}{(1+\beta' I_x)^2}\mathrm{e}^{-\alpha z}\,.$$

The integral along the laser length must vanish according to (9). After some algebra, we find:

$$\frac{\mathrm{d}\mathcal{A}}{\mathcal{A}} = \frac{(1+\delta)(1+\beta' I_x)^2+\beta'^2(1-\delta)(1+I_x)^2}{(1+\delta)(1+I_x)(1+\beta' I_x)^2+\beta'(1-\delta)(1+\beta' I_x)(1+I_x)^2}\,\mathrm{d}I_x. \tag{20}$$

Equation (20) can be directly integrated from the threshold $\mathcal{A}_x^{\mathrm{th}}$ to $\mathcal{A}$. Its solution is :

$$\frac{\mathcal{A}}{\mathcal{A}_x^{\mathrm{th}}} = \frac{(1+\beta'+\delta(1-\beta'))(1+I_x)(1+\beta' I_x)}{1+\beta'+\delta(1-\beta')+2\beta' I_x}\,. \tag{21}$$

Relations (21) and (18) finally allow us to express I_x as a function of the pumping parameter:

$$I_x = \frac{\mathcal{A}}{2L_{\mathrm{p}}\Gamma_x} - \frac{1}{1-\epsilon'} - \sqrt{\left(\frac{\mathcal{A}}{2L_{\mathrm{p}}\Gamma_x}+\frac{\epsilon'}{1-\epsilon'}\right)^2 - \frac{\epsilon'(1-\delta)\mathcal{A}}{(1-\epsilon')L_{\mathrm{p}}\Gamma_x}}. \tag{22}$$

The last step is the evaluation of $I_x(l)$ using the relations:

$$I_x = I_x^+(l) + I_x^-(l) = (1+R_{2x})I_x^+(l)\,,$$

$$I_x^{\mathrm{out}}(l) = (1-R_{2x})I_x^+(l)\,.$$

The last relation allows us to find the output intensity:

$$I_x^{\mathrm{out}}(l) = \frac{1-R_{2x}}{1+R_{2x}}\left[\frac{\mathcal{A}}{2L_{\mathrm{p}}\Gamma_x} - \frac{1}{1-\epsilon'} - \sqrt{\left(\frac{\mathcal{A}}{2L_{\mathrm{p}}\Gamma_x}+\frac{\epsilon'}{1-\epsilon'}\right)^2 - \frac{\epsilon'(1-\delta)\mathcal{A}}{(1-\epsilon')L_{\mathrm{p}}\Gamma_x}}\right]. \tag{23}$$

3.2 Bimode solutions : $\mathcal{A} > \mathcal{A}_y^{\mathrm{th}}$

We derive in this section approximate analytical expressions for the threshold for the weak mode and for the intensities above this second threshold. Let us first introduce an important parameter, called the cavity loss anisotropy, Δ which include both localized and distributed loss anisotropies. Δ is given by:

$$\Delta = \frac{\Gamma_y-\Gamma_x}{\Gamma_y+\Gamma_x}\,,$$

where Γ_x is given by (18c) and Γ_y represents the total losses for mode Y:

$$\Gamma_y = (1+\gamma) - \frac{1}{2l}\ln\left[(1-t_1)(1-t_2)R_1R_2\right]\,.$$

As a consequence of the use of Δ, we have to introduce the mean losses coefficient, $\Gamma = (\Gamma_y+\Gamma_x)/2$, in order to express Γ_x and Γ_y as a function of Δ:

$$\Gamma_x = (1-\Delta)\Gamma\,,$$

$$\Gamma_y = (1+\Delta)\Gamma\,.$$

Δ and Γ can be expressed as a function of both localized and distributed loss anisotropies:

$$\Delta = \frac{4\gamma l - \ln\left[\frac{1-t_1}{1+t_1}\frac{1-t_2}{1+t_2}\right]}{4l - \ln\left[(1-t_1^2)(1-t_2^2)R_1^2R_2^2\right]}\,,$$

$$\Gamma = 1 - \frac{1}{4l}\ln\left[(1-t_1^2)(1-t_2^2)R_1^2R_2^2\right]\,.$$

Let us note that for weak localized loss anisotropy, i.e. $t_{1,2}^2 \ll 1$, Δ and Γ may be written as:

$$\Delta = \frac{4\gamma l - \ln\left[\frac{1-t_1}{1+t_1}\frac{1-t_2}{1+t_2}\right]}{4l - \ln\left[R_1^2R_2^2\right]}\,,$$

$$\Gamma = 1 - \frac{1}{2l}\ln\left[R_1R_2\right]\,.$$

The threshold for the Y mode is derived in Appendix A and its expression is:

$$\mathcal{A}_y^{\mathrm{th}} = L_{\mathrm{p}}\Gamma\frac{(1+\epsilon')(\epsilon'^2-\Delta^2)}{\epsilon'^2-\delta\epsilon'(1-\Delta)-\Delta}\,.$$

The output intensities are (Appendix B):

$$I_x^{\mathrm{out}}(l) = \frac{1-(1+t_2)R_2}{1+(1+t_2)R_2}\frac{1+\epsilon'}{2} \times\left[\frac{\epsilon'^2+\delta\epsilon'(1+\Delta)+\Delta}{(1+\epsilon')(\epsilon'^2-\Delta^2)}\frac{\mathcal{A}}{L_{\mathrm{p}}\Gamma}-1\right], \tag{24a}$$

$$I_y^{\mathrm{out}}(l) = \frac{1-(1-t_2)R_2}{1+(1-t_2)R_2}\frac{1+\epsilon'}{2} \times\left[\frac{\epsilon'^2-\delta\epsilon'(1-\Delta)-\Delta}{(1+\epsilon')(\epsilon'^2-\Delta^2)}\frac{\mathcal{A}}{L_{\mathrm{p}}\Gamma}-1\right]. \tag{24b}$$

Previous results have been obtained assuming that the strong mode is polarized along the x axis. It can be easily shown using relation (A.3) that this is the case if $\delta\epsilon' > -\Delta$. In the opposite case where $\delta\epsilon' < -\Delta$, the strong mode is polarized along the y axis. The single-mode solution, in the range $\mathcal{A}_y^{\mathrm{th}} < \mathcal{A} < \mathcal{A}_x^{\mathrm{th}}$ is then slightly different from relation (23). The bimode solution above the second threshold ($\mathcal{A}_x^{\mathrm{th}}$) has the same analytical expression as the bimode solution (24) obtained in the case of a strong mode polarized along x. A summary of the analytical expressions of output intensities and thresholds is given in Appendix C.

4 Discussion

4.1 Operating regime diagram

As mentioned above, the respective values of the thresholds associated to the two polarization eigenmodes depend upon both the passive and pump-induced anisotropies. In order to have a synthetic view of the different operating regimes (single-mode X or Y, bimode X > Y or Y > X) we show in Fig. 5 the boundaries between the different regimes in the plane (Δ, δ). The straight line (solid curve) corresponds to the exact values of the total passive loss anisotropy Δ which compensate the gain anisotropy δ, i.e. $\delta\epsilon' = -\Delta$. In this case, intensities and thresholds of both modes X and Y are equal. For higher Δ or δ, the strong mode is polarized along the x axis and the curve, whose equation is $\Delta = \epsilon'(\epsilon' - \delta)/(1 - \delta\epsilon')$ corresponds to the limit above which the Y mode cannot oscillate. In this case the numerical value of the threshold of the Y mode becomes negative resulting in a single-polarization operating regime whatever the pumping ratio. In Nd-doped fiber lasers, this is the case when, for example, a prism is inserted in the cavity [23]. Because of the symmetry of the operating regime diagram, the same arguments may be applied in the half-plan below the straight line for mode Y. In this case the equation of the boundary curve is $\Delta = -\epsilon'(\epsilon' + \delta)/(1 + \delta\epsilon')$.

For a given cross-saturation parameter for the pump (β), which fixes the value of ϵ, δ is varied in the range $[-\epsilon, +\epsilon]$ simply by a rotation of the pump-input polarization angle, see (2). Note that since β ranges from zero to unity, δ is bounded by ± 1. On the other hand for a fixed pump polarization angle, the total passive gain anisotropy, Δ, can be changed by either a tilt of one mirror or a variation of the fiber length. In addition, previous works have demonstrated the stability of these different operating regimes under the mean-field approximation [10].

4.2 Comparison of analytical and numerical results

As a first test for the analytical results, we can compare them with the exact numerical solutions giving the evolution of the output intensities versus the pumping ratio. An example of laser characteristics is given in Fig. 6. A very good agreement is obtained in this case (one cannot distinguish the analytical case from the numerical one). The values of the parameters used are $\alpha = 100$, $R_1 = 1$, $R_2 = 0.8$, $l = 0.1$, $t_1 = 0.005$, $t_2 = 0.005$, $\gamma = 0.005$ ($\rightarrow \Delta = 0.026$), $\epsilon = 0.01$, and $\epsilon' = 0.33$. These parameters lie in the range for which the initial assumption is valid and will be used hereafter except when specified. We also have verified that the range of validity of the analytical results, for both the general model and the single-mode model, is the same.

As in the previous section, we investigate the evolution of the output intensities for the two polarized eigenmodes as functions of the fiber length (Fig. 7a) and the output mirror reflectivity (Fig. 7b). The results are given in Fig. 7 for both the exact numerical results (solid lines) and the approximate analytical results (dotted lines). Beyond the fact that

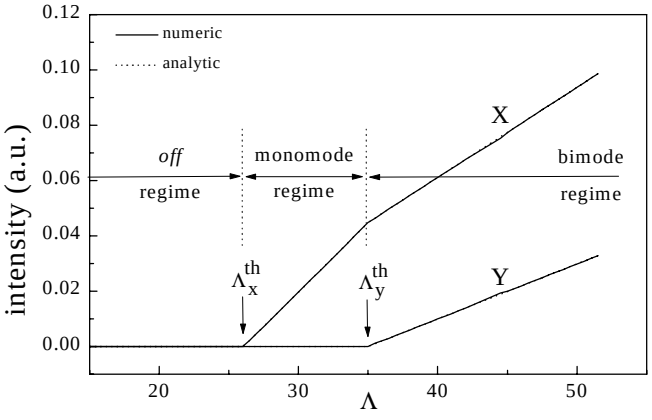

Fig. 6. Evolution of the output intensities I_x and I_y versus the pumping parameter. Analytic (*dotted*) and numerical solutions (*solid*) coincide so well they cannot be distinguished

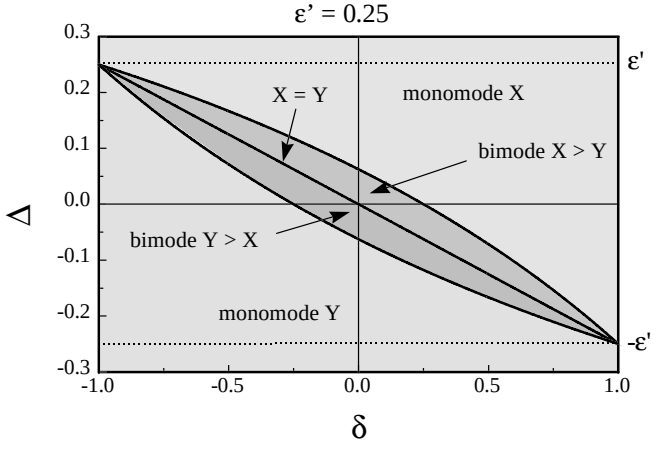

Fig. 5. Operating regime diagram in the plane (δ, Δ). The parameter used is $\beta' = 0.6$ ($\epsilon' = 0.25$)

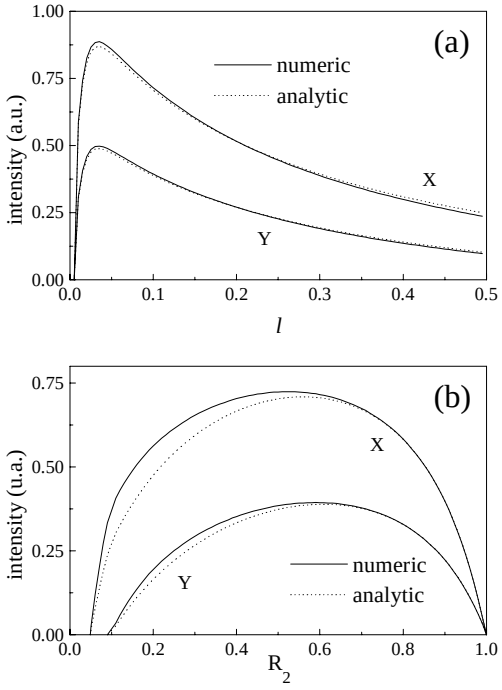

Fig. 7. **a** $I_{x,y} = f(l)$ analytic (*dotted*) and numerical (*solid*) solutions. **b** $I_{x,y} = f(R_2)$ analytic (*dotted*) and numerical (*solid*) solutions

there is a good agreement, especially for short fiber lengths and high output mirror reflectivities, our results show essentially two features. First, there exists an optimum fiber length, for the two modes, which maximizes the output intensities, this is a direct consequence of a decreasing unsaturated gain and distributed losses and this result is well known for a single-mode laser [2, 20]. Moreover, the old problem of output coupling optimization [2] reveals new results since the optimum value of R_2 is different for the two modes. This is connected with the various dichroic losses experienced by the two eigenmodes.

4.3 Influence of fiber length

In addition to previous results related to optimization problems, pump-polarization effects can also be investigated with our formalism, in particular the influence of the fiber length on the evolution of the thresholds versus the pump-input polarization angle ϕ_0. Recall that we have considered a linearly polarized pump field. The evolution of Λ_x^{th} and Λ_y^{th} versus the angle ϕ_0 is a well-known result both experimentally and theoretically [10, 18]. In contrast with [10] our model allows us to take into account length effects. Indeed, let us consider a localized gain anisotropy on the output mirror which favors the mode polarized along the x axis ($t_2 = 0.01$) and a distributed gain anisotropy which favors the Y mode ($\gamma = -0.02$). One can reasonably expect that what fixes the strong mode is the combination of the gain anisotropy and the total passive loss anisotropy. Figure 8 gives the evolution of Δ as a function of the fiber length l. The effect of the passive loss anisotropy is as follows: for short lengths $\Delta > 0$ and the X mode is favored, whereas for increasing lengths Δ becomes negative, resulting in a lower threshold for the Y mode. These facts are verified in Fig. 9a–c which give the evolution of Λ_x^{th} and Λ_y^{th} versus the angle ϕ_0 for three increasing lengths: (a) $l = 0.1$, (b) $l = 0.275$, and (c) $l = 0.5$. In all cases, the threshold values are normalized with respect to the lowest threshold value. Figure 9 shows that the range for which $\Lambda_x^{\text{th}} > \Lambda_y^{\text{th}}$ increases for increasing lengths. This is a direct consequence of the evolution of the total passive loss anisotropy. Moreover, note that, although for short lengths $\Delta > 0$, there exists a range of pump-input polarization angles (in the vicinity of $\phi_0 = \pi/2$)

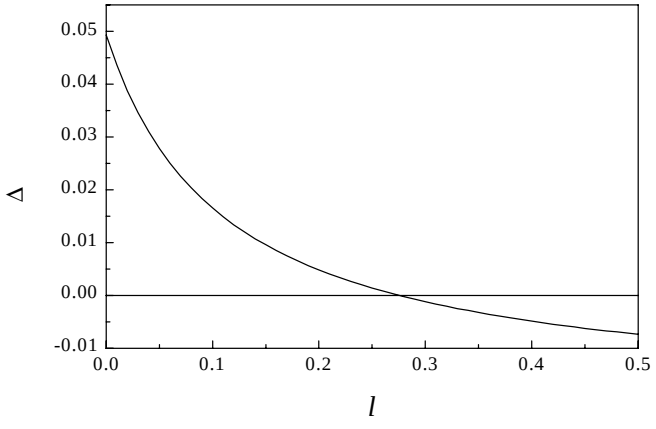

Fig. 8. Evolution of the total passive loss anisotropy versus the fiber length

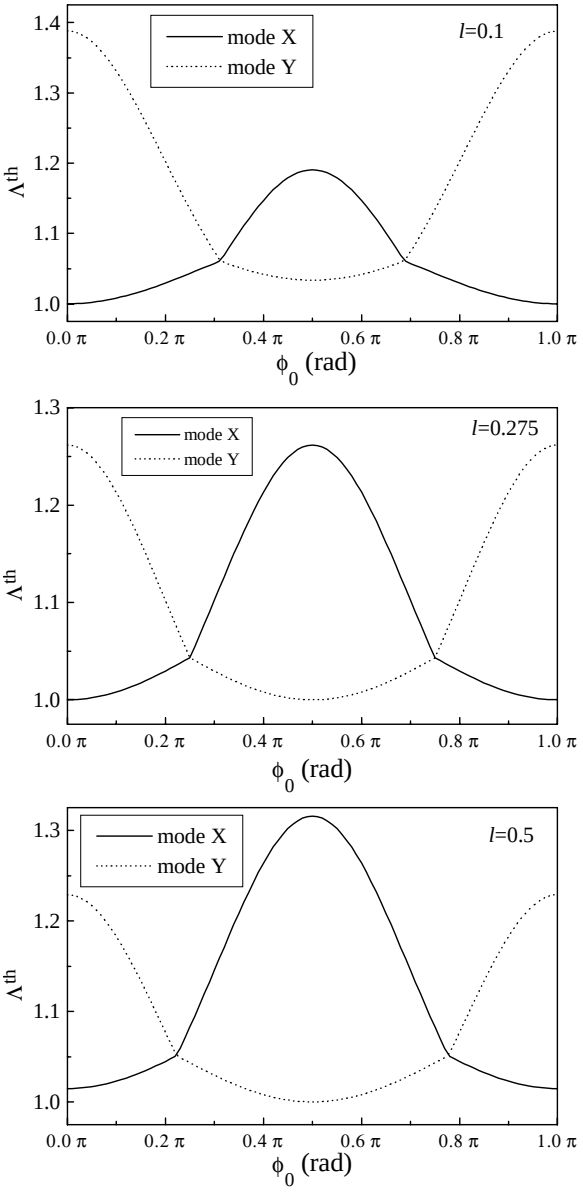

Fig. 9. Evolution of the thresholds of the two modes versus the pump polarization angle for different fiber lengths. The *solid* (*dotted*) *line* corresponds to the X mode (Y mode)

for which $\Lambda_x^{\text{th}} > \Lambda_y^{\text{th}}$. This is due to the competing effect between the pump-induced anisotropy and the total passive loss anisotropy. In particular, when the pump polarization is parallel to the y axis, the Y-mode threshold is always lower than the threshold of the X mode whatever the active medium length (for the parameters used, of course). Different evolutions may be observed for lower values of the pump-induced anisotropy.

There exists a particular fiber length ($l_0 = 0.275$ for our parameters) for which Δ vanishes (see Fig. 8). Its analytical expression is:

$$l_0 = \frac{1}{4\gamma} \ln \left[\frac{(1-t_1)(1-t_2)}{(1+t_1)(1+t_2)} \right] . \tag{25}$$

Relation (25) shows that such length exists if distributed and localized loss anisotropy have opposite signs. Under such

conditions and for this fiber length the evolution of $\Lambda_x^{\rm th}$ and $\Lambda_y^{\rm th}$ is the same with merely a $\pi/2$ angle shift resulting from the periodicity of the gain anisotropy. This means that any mode is favored by the passive loss anisotropy.

For vanishing fiber lengths, the asymptotic value of the passive loss anisotropy is:

$$\Delta_0 = \frac{\ln\left[\frac{(1-t_1)(1-t_2)}{(1+t_1)(1+t_2)}\right]}{\ln\left[(1-t_1^2)(1-t_2^2)R_1^2R_2^2\right]}\,.$$

Or, for weak loss anisotropies:

$$\Delta_0 = \frac{\ln\left[\frac{(1-t_1)(1-t_2)}{(1+t_1)(1+t_2)}\right]}{\ln\left[R_1^2R_2^2\right]}\,.$$

In our case we have $\Delta_0 \approx 0.045$ which is positive thus resulting in a strong mode polarized along the x axis.

On the other hand for extremely long fibers, the asymptotic value of the passive loss anisotropy is:

$$\Delta_\infty = \gamma\,.$$

In our case $\Delta_\infty = -0.02$ is negative and the strong mode is polarized along the y axis.

5 Conclusions

This paper has been devoted to the investigation of the combined effect of the length, passive loss anisotropy, and gain anisotropy on the steady-state properties of a fiber laser. The formalism used is a generalization of Rigrod's theory to the case of a bipolarized laser. This approach is well adapted to introduce the characteristics of the Nd-doped fiber laser. Indeed, we have taken into account an exponentially decreasing unsaturated gain along the fiber (proportional to the variations of the pump intensity), a localized loss anisotropy on the mirrors, and a distributed loss anisotropy. The general problem only admits numerical solutions. In order to obtain analytical results we have proposed an assumption, less restrictive than the mean-field approximation, which consists of considering that the local average intensity remains constant over the fiber length, whereas the forward and backward intensities are not uniform. In order to validate our hypothesis, we have investigated the simple case of a single-mode laser. The results have shown that, depending on the desired agreement, there exists some range of parameters (fiber length and output mirror reflectivity) for which the approximation is valid. Typically, the agreement is very good for short fiber lengths and high output reflection coefficients.

Furthermore, the general model has been investigated in view of determining the combined effects of the pump-input polarization angle and the fiber length on the thresholds evolution of the two eigenmodes. The various anisotropies considered lead to a loss of symmetry between the two polarized eigenmodes. Therefore, one has to distinguish different possible situations: the strong mode can be polarized along the x or y axis. In addition, the existence of the second threshold (associated with the weak mode) also depends on the respective values of the anisotropies. Analytical expressions for both the thresholds and the output intensities have been obtained in all cases, using the same approximation as in the single-mode case. A good agreement has been obtained between the exact numerical and approximate analytical solutions for the laser characteristic and for the evolution of the output intensities versus both the fiber length and output mirror reflectivity.

The evolution of the thresholds versus the pump-input polarization angle for increasing fiber lengths has been studied using the analytical expressions. We have demonstrated that these evolutions depend on the competing effect between the gain anisotropy and the total passive loss anisotropy. The latter represents a global parameter including localized and distributed loss anisotropy. We have shown that for short fiber lengths the total passive loss anisotropy is mainly imposed by the localized processes, whereas for high lengths it is mainly monitored by distributed loss anisotropy. These results could be easily expected from simple physical and intuitive arguments.

The analytical results obtained in this paper are of great interest for the experimental determination of pump-induced, localized and distributed anisotropies in fiber lasers but also in the more general case of end-pumped solid-state lasers.

Acknowledgements. The authors are very grateful to Dr. B. Meziane for stimulating discussions and his comments on the manuscript.

Appendix A: Threshold for the weak mode

In this appendix, the threshold for the Y mode is derived. The strong (weak) mode is polarized along the x axis (y axis). Let us consider the gain experienced by the Y mode at its lasing threshold (the saturation by the X mode has to be taken into account):

$$G_y(z) = \frac{1}{2}\frac{(1-\delta)\Lambda_y^{\rm th}{\rm e}^{-\alpha z}}{1+\beta'(I_x^+ + I_x^-)} + \frac{1}{2}\beta'\frac{(1+\delta)\Lambda_y^{\rm th}{\rm e}^{-\alpha z}}{1+I_x^+ + I_x^-}\,,$$

where I_x^+ and I_x^- are the forward and backward intensities of the mode X for $\Lambda = \Lambda_y^{\rm th}$. Let:

$$I_x^0 = I_x^+(\Lambda_y^{\rm th}) + I_x^-(\Lambda_y^{\rm th})\,.$$

The oscillation condition is:

$$R_{1y}R_{2y}\exp\left[2\int_0^l\left(\left(\frac{1-\delta}{1+\beta' I_x^0}+\beta'\frac{1+\delta}{1+I_x^0}\right)\frac{\Lambda_y^{\rm th}}{2}{\rm e}^{-\alpha z}-1-\gamma\right){\rm d}z\right] = 1\,. \qquad \text{(A.1)}$$

Equation (A.1) leads to:

$$\frac{\Lambda_y^{\rm th}}{2}\frac{(1-\delta)(1+I_x^0)+\beta'(1+\delta)(1+\beta' I_x^0)}{(1+I_x^0)(1+\beta' I_x^0)} = L_{\rm p}\Gamma_y\,. \qquad \text{(A.2)}$$

I_x^0 is calculated from relation (22) at $\Lambda = \Lambda_y^{\rm th}$. The inclusion of the latter expression in (A.2) leads, after some cumbersome algebra, to an equation for the second threshold:

$$\frac{\Lambda_y^{\rm th}}{\Lambda_x^{\rm th}} = \frac{1+\delta\epsilon'}{1-\Delta}\frac{\epsilon'^2-\Delta^2}{\epsilon'^2-\delta\epsilon'(1-\Delta)-\Delta}\,. \qquad \text{(A.3)}$$

Appendix B: Output intensities above the second threshold

In order to derive analytical expressions for $I_x^+(l)$ and $I_y^+(l)$, we assume that :

$$I_{x,y} = I_x^+(z) + I_y^+(z) = C^{\rm st}\,. \tag{B.1}$$

The saturated gains can be written:

$$G_x(z) = \frac{1}{2}\frac{(1+\delta)\Lambda e^{-\alpha z}}{1+I_x+\beta' I_y} + \frac{1}{2}\beta'\frac{(1-\delta)\Lambda e^{-\alpha z}}{1+\beta' I_x+I_y}\,, \tag{B.2a}$$

$$G_y(z) = \frac{1}{2}\frac{(1-\delta)\Lambda e^{-\alpha z}}{1+\beta' I_x+I_y} + \frac{1}{2}\beta'\frac{(1+\delta)\Lambda e^{-\alpha z}}{1+I_x+\beta' I_y}\,. \tag{B.2b}$$

The derivative versus the pump parameter yields:

$$\frac{{\rm d}G_x(z)}{{\rm d}\Lambda} = \frac{1+\delta}{2}\frac{1+I_x+\beta' I_y-\Lambda\left(\frac{{\rm d}I_x}{{\rm d}\Lambda}+\beta'\frac{{\rm d}I_y}{{\rm d}\Lambda}\right)}{(1+I_x+\beta' I_y)^2}e^{-\alpha z} + \beta'\frac{1-\delta}{2}\frac{1+\beta' I_x+I_y-\Lambda\left(\beta'\frac{{\rm d}I_x}{{\rm d}\Lambda}+\frac{{\rm d}I_y}{{\rm d}\Lambda}\right)}{(1+\beta' I_x+I_y)^2}e^{-\alpha z}, \tag{B.3a}$$

$$\frac{{\rm d}G_y(z)}{{\rm d}\Lambda} = \beta'\frac{1+\delta}{2}\frac{1+I_x+\beta' I_y-\Lambda\left(\frac{{\rm d}I_x}{{\rm d}\Lambda}+\beta'\frac{{\rm d}I_y}{{\rm d}\Lambda}\right)}{(1+I_x+\beta' I_y)^2}e^{-\alpha z} + \frac{1-\delta}{2}\frac{1+\beta' I_x+I_y-\Lambda\left(\beta'\frac{{\rm d}I_x}{{\rm d}\Lambda}+\frac{{\rm d}I_y}{{\rm d}\Lambda}\right)}{(1+\beta' I_x+I_y)^2}e^{-\alpha z}. \tag{B.3b}$$

The previous expressions are integrated along the laser length and matched to zero. This procedure leads to the following expressions:

$$1+I_x+\beta' I_y-\Lambda\left(\frac{{\rm d}I_x}{{\rm d}\Lambda}+\beta'\frac{{\rm d}I_y}{{\rm d}\Lambda}\right)=0\,, \tag{B.4a}$$

$$1+\beta' I_x+I_y-\Lambda\left(\beta'\frac{{\rm d}I_x}{{\rm d}\Lambda}+\frac{{\rm d}I_y}{{\rm d}\Lambda}\right)=0\,. \tag{B.4b}$$

The previous relations lead to:

$$\frac{{\rm d}\Lambda}{\Lambda} = \frac{1+\beta'}{1+(1+\beta')I_x}\,{\rm d}I_x\,, \tag{B.5a}$$

$$\frac{{\rm d}\Lambda}{\Lambda} = \frac{1+\beta'}{1+(1+\beta')I_y}\,{\rm d}I_y\,. \tag{B.5b}$$

The integration of (B.5) from $\Lambda_y^{\rm th}$ to Λ yields :

$$I_x = \frac{1}{1+\beta'}\left[\left(1+(1+\beta')I_x^0\right)\frac{\Lambda}{\Lambda_y^{\rm th}}-1\right], \tag{B.6a}$$

$$I_y = \frac{1}{1+\beta'}\left[\frac{\Lambda}{\Lambda_y^{\rm th}}-1\right], \tag{B.6b}$$

where I_x^0 is the particular value of I_x for $\Lambda=\Lambda_y^{\rm th}$.
The output intensities are easily deduced from (B.6).

Appendix C: Summary of analytical results

- *Single-mode operation with X:*

This occurs when $\epsilon'\Delta > -\delta$ and either $\Lambda < \Lambda_y^{\rm th}$ or $\Delta > \epsilon'(\epsilon'-\delta)/(1-\delta\epsilon')$ whatever Λ.
Output intensity:

$$I_x^{\rm out}(l) = \frac{1-(1+t_2)R_2}{1+(1+t_2)R_2}\left[\frac{\Lambda}{2(1-\Delta)\Gamma L_{\rm p}} - \frac{1}{1-\epsilon'} - \sqrt{\left(\frac{\Lambda}{2(1-\Delta)\Gamma L_{\rm p}}+\frac{\epsilon'}{1-\epsilon'}\right)^2 - \frac{\epsilon'(1-\delta)\Lambda}{(1-\epsilon')(1-\Delta)\Gamma L_{\rm p}}}\right].$$

Threshold:

$$\Lambda_x^{\rm th} = \Gamma L_p(1-\Delta)\frac{1+\epsilon'}{1+\delta\epsilon'}\,.$$

- *Single-mode operation with Y:*

This occurs when $\epsilon'\Delta < -\delta$ and either $\Lambda < \Lambda_x^{\rm th}$ or $\Delta < -\epsilon'(\epsilon'+\delta)/(1+\delta\epsilon')$ whatever Λ.
Output intensity:

$$I_y^{\rm out}(l) = \frac{1-(1-t_2)R_2}{1+(1-t_2)R_2}\left[\frac{\Lambda}{2(1+\Delta)\Gamma L_{\rm p}} - \frac{1}{1-\epsilon'} - \sqrt{\left(\frac{\Lambda}{2(1+\Delta)\Gamma L_{\rm p}}+\frac{\epsilon'}{1-\epsilon'}\right)^2 - \frac{\epsilon'(1+\delta)\Lambda}{(1-\epsilon')(1+\Delta)\Gamma L_{\rm p}}}\right].$$

Threshold:

$$\Lambda_y^{\rm th} = \Gamma L_{\rm p}(1+\Delta)\frac{1+\epsilon'}{1-\delta\epsilon'}\,.$$

- *bimode operation:*

This occurs when $-\epsilon'(\epsilon'+\delta)/(1+\delta\epsilon') < \Delta < \epsilon'(\epsilon'-\delta)/(1-\delta\epsilon')$ and $\Lambda >$ treshold of the weak mode.
Output intensities:

$$I_x^{\rm out}(l) = \frac{1-(1+t_2)R_2}{1+(1+t_2)R_2}\frac{1+\epsilon'}{2}\left[\frac{\epsilon'^2+\delta\epsilon'(1+\Delta)+\Delta}{(1+\epsilon')(\epsilon'^2-\Delta^2)}\frac{\Lambda}{\Gamma L_{\rm p}}-1\right],$$

$$I_y^{\rm out}(l) = \frac{1-(1-t_2)R_2}{1+(1-t_2)R_2}\frac{1+\epsilon'}{2}\left[\frac{\epsilon'^2-\delta\epsilon'(1-\Delta)-\Delta}{(1+\epsilon')(\epsilon'^2-\Delta^2)}\frac{\Lambda}{\Gamma L_{\rm p}}-1\right].$$

Threshold:
If $\epsilon'\Delta > \delta$, the strong mode is along x:

$$\Lambda_y^{\rm th} = L_{\rm p}\Gamma\frac{(1+\epsilon')(\epsilon'^2-\Delta^2)}{\epsilon'^2-\delta\epsilon'(1-\Delta)-\Delta}\,.$$

If $\epsilon'\Delta < \delta$, the strong mode is along y:

$$\Lambda_x^{\rm th} = L_{\rm p}\Gamma\frac{(1+\epsilon')(\epsilon'^2-\Delta^2)}{\epsilon'^2+\delta\epsilon'(1+\Delta)+\Delta}\,.$$

References

1. A. Yariv: *Quantum Electronics*, 3rd edn. (Wiley, New York 1989)
2. W.W. Rigrod: J. Appl. Phys. **34**, 2602 (1963); W.W. Rigrod: IEEE J. Quantum. Electron. **14**, 377 (1978)
3. S. Longhi: J. Opt. Soc. Am. B **11**, 1098 (1994)
4. M.J.F. Digonnet: IEEE J. Quantum. Electron. **10**, 1788 (1990)
5. F. Sanchez, B. Meziane, T. Chartier, G. Stéphan, P.L. François: Appl. Opt. **34**, 7674 (1995)
6. K. Wiesenfeld, C. Bracikowski, G. James, R. Roy: Phys. Rev. Lett. **65**, 1749 (1990)
7. J. Martin-Regalado, M. SanMiguel, N.B. Abraham, F. Prati: Opt. Lett. **21**, 351 (1996)
8. P. Besnard, F. Robert, M.L. Chares, G. Stéphan: Phys. Rev. A **56**, 3191 (1997)
9. S. Bielawski, D. Derozier, P. Glorieux: Phys. Rev. A **46**, 2811 (1992)
10. R. Leners, G. Stéphan: Quantum. Semiclass. Opt. **7**, 757 (1995)
11. F. Sanchez, G. Stéphan: Phys. Rev. E **53**, 2110 (1996)
12. R.J. Ballagh, N.J. Mulgan: Phys. Rev. A **52**, 4945 (1995)
13. A.D. May, G. Stéphan: J. Opt. Soc. Am. B **6**, 2355 (1989)
14. A.M. Kulminskii, R. Vilaseca, R. Corbalan: J. Mod. Opt. **42**, 2295 (1995)
15. M. Ikezouhene, B. Meziane, G. Stéphan: Opt. Quantum. Electron. **28**, 1029 (1996)
16. T. Chartier, F. Sanchez, G. Stéphan: Appl. Phys. B **70**, 23 (2000), (DOI) 10.1007/s003409900137
17. H. Statz, G. DeMars: J. Appl. Phys. **35**, 1377 (1964)
18. R. Leners, P.L. François, G. Stéphan: Opt. Lett. **19**, 275 (1994)
19. H.J. Carmichael: Opt. Acta **27**, 147 (1980)
20. E. Puig Maldonado, N. Dias Vieira, Jr.: J. Opt. Soc. Am. B **12**, 2482 (1995)
21. G.M. Schindler: IEEE J. Quantum. Electron. **16**, 546 (1980)
22. L. Zenteno: IEEE J. Light. Tech. **11**, 1435 (1993)
23. T. Chartier, P. LeBoudec, F. Sanchez, E. Delevaque, R. Leners, P.L. François, G. Stéphan: Opt. Lett. **18**, 355 (1993)